Dynamics of heavy particles in a Burgers vortex

B. Marcu, E. Meiburg,[a] and P. K. Newton
Department of Aerospace Engineering, University of Southern California, Los Angeles, California 90089-1191

(Received 15 July 1994; accepted 4 October 1994)

This paper presents a linear stability analysis as well as some numerical results for the motion of heavy particles in the flow field of a Burgers vortex, under the combined effects of particle inertia, Stokes drag, and gravity. By rendering the particle motion equations dimensionless, the particle Stokes number, a Froude number, and a vortex Reynolds number are obtained as the governing three parameters. In the absence of gravity, the vortex center represents a stable equilibrium point for particles up to a critical value of the Stokes number, as the inward drag overcomes the destabilizing centrifugal force on the particle. Particles exceeding the critical Stokes number value asymptotically approach closed circular orbits. Under the influence of gravity, one or three equilibrium points appear away from the vortex center. Both their locations and their stability characteristics are derived analytically. These stability characteristics can furthermore be related to the nature of the critical points in a related directional force field. These findings are expected to be applicable to the coupling between the small-scale turbulent flow structures and the motion of suspended particles. © *1995 American Institute of Physics.*

I. INTRODUCTION

An important goal in two-phase flow research is the development of simple yet comprehensive models for the interaction of small drops and solid particles with turbulent flow fields. Towards this end, the computational[1–3] and experimental[4–7] investigations of the influence of the two-dimensional large-scale flow structures on the overall particle dispersion represent an important step. A common observation in all of the above investigations has been the ejection of particles from vortex centers, along with their accumulation in regions near stagnation points. The obvious explanation for the particle ejection from strong vortical regions is the absence, in two-dimensional flows, of a force that could counteract the outwardly directed centrifugal force.

Further important information on the dynamics of particles in turbulent flow fields is obtained from the statistical data provided by direct Navier–Stokes simulations with passive and active particles.[8–14] As Wang and Maxey point out, quantities such as the settling velocity under gravity and local accumulation properties of the particles are a function of small-scale turbulence processes rather than the large eddies. Their simulations demonstrate that the successful design of two-phase turbulence models will eventually have to be based on a thorough understanding of the dynamical interplay between the inertial, drag, gravitational, and other forces acting on the particles and the small-scale vortical structures of the turbulent flow field. In this regard, recent findings from direct Navier–Stokes simulations of turbulent flows[15,16] provide evidence that extensionally strained concentrated tube-like vortices play a prominent role in fully developed turbulence.

Based on these and other observations, Ashurst[17] suggests that much of the dynamics of turbulence can be understood by regarding it as a collection of Burgers vortices.[18] Ashurst furthermore points out that for a particle moving in the field of a Burgers vortex, the drag force created by the radially inward fluid motion can balance the centrifugal force, thereby preventing the particle from being ejected. A similar argument concerning a balance between the centrifugal and drag forces was put forward by Maxworthy.[19] Given the important role that the small scales play in the interaction between particles and turbulence, and the prominence of Burgers vortex-like structures among these small scales, an investigation of the dynamics of heavy particles in the field of a Burgers vortex will provide useful information towards an understanding of two-phase turbulence. In the following, we will establish the governing nondimensional equations and parameters, and subsequently analyze separately the cases without and with gravity.

II. FLOW MODEL AND GOVERNING EQUATIONS

The fluid flow model is a steady Burgers vortex with the axial, radial, and circumferential velocity components, respectively,

$$v_z = 2\sigma z,$$
$$v_r = -\sigma r, \tag{1}$$
$$v_\theta = \frac{\Gamma}{2\pi r}\left[1-\exp\left(-\frac{r^2}{2\delta^2}\right)\right].$$

Here σ denotes the strain, and Γ represents the circulation of the vortex, whose core size $\delta = \sqrt{\nu/\sigma}$ is determined by the balance of strain and viscous diffusion ν.

By choosing δ as a characteristic length, and Γ/δ as the characteristic velocity, the nondimensional flow field has the form

[a]Corresponding author: E. Meiburg, Department of Aerospace Engineering, University of Southern California, Los Angeles, CA 90089-1191. Phone: (213) 740–5376, Fax: (213) 740–7774.

 1070-6631/95/7(2)/400/11/$6.00

$$v_z=2Az,$$
$$v_r=-Ar, \tag{2}$$
$$v_\theta=\frac{1}{2\pi r}\left[1-\exp\left(-\frac{r^2}{2}\right)\right].$$

Here $A=\sigma\delta^2/\Gamma=\nu/\Gamma$ is the nondimensional strain parameter, $1/A$ is also known as the vortex Reynolds number. Our interest focuses on the two-dimensional particle dynamics in the r, θ plane, in which the velocity field in Cartesian coordinates becomes

$$u=-Ax-\frac{y}{2\pi r^2}\left[1-\exp\left(-\frac{r^2}{2}\right)\right],$$
$$v=-Ay+\frac{x}{2\pi r^2}\left[1-\exp\left(-\frac{r^2}{2}\right)\right], \tag{3}$$
$$r^2=x^2+y^2.$$

In studying the particle motion, we limit ourselves to the dilute regime, in which both the particles' effect on the fluid motion, as well as the particle–particle interaction is neglected. In most situations involving solid particles or liquid drops in gaseous flows, the particle motion will be determined by the effects of inertia, viscous drag, and gravity,[4] with all other forces being at least one order of magnitude smaller. The motion for a small, spherical, rigid particle of diameter d, density ρ_p and velocity $\mathbf{V}=(u_p,v_p)$ in a fluid with density ρ_f and velocity $\mathbf{U}=(u_f,v_f)$, then is determined by the nondimensional equations[20]

$$\mathbf{V}=\frac{d\mathbf{x_p}}{dt}, \tag{4}$$

$$\frac{d\mathbf{V}}{dt}=\frac{1}{\mathrm{St}}(\mathbf{U}|_{\mathbf{x}=\mathbf{x}_p}-\mathbf{V})+\frac{1}{\mathrm{Fr}^2}\mathbf{e_g}, \tag{5}$$

where Stokes' drag law is employed. Here $\mathbf{x_p}$ denotes the instantaneous position of the particle, $\mathbf{U}$ is the fluid velocity as given by (3) at the location $\mathbf{x_p}$ while $\mathbf{e_g}$ represents the unit vector in the direction of the gravity vector's projection into the r, θ plane. It should be pointed out that the particle motion in the axial direction is decoupled from that in the r, θ plane, so that it does not affect the stability, or the r or θ components of the equilibrium position. The parameters

$$\mathrm{St}=\frac{d^2}{18}\frac{\rho_p}{\rho_f}\frac{\sigma\Gamma}{\nu^2} \tag{6}$$

and

$$\mathrm{Fr}=\frac{\sigma^{3/4}\Gamma}{\nu^{3/4}\sqrt{g}} \tag{7}$$

are the Stokes and Froude number, respectively. Here g is the length of the projection of the gravitational acceleration vector $\mathbf{g}$ on the r, θ plane. The following analysis is hence valid for arbitrary orientations of the vortex axis with respect to the direction of gravity. Crowe *et al.*[1] interpret the Stokes number as the ratio of the aerodynamic response time of the particle $\tau_A=\rho_p d^2/18\mu$ to the time scale associated with the fluid motion, which for the present study is $\tau=\nu/\Gamma\sigma$. Small values of the Stokes parameter may be regarded as describing either very light particles or a very viscous fluid, in both cases the particle behavior being dominated by the viscous forces. In contrast, large values of the Stokes parameter describe either heavy particle or a less viscous fluid, with particle behavior being dominated by inertial forces. The Froude number expresses in nondimensional form the relative importance of inertial forces and gravitational forces for the particle motion. Large Froude numbers describe inertia dominated particle motion, for which gravity is not important and the behavior of the particle is determined merely by the ratio between the viscous and inertial forces given by the Stokes number. As the Froude number decreases, gravity becomes more important for the dynamical behavior of the particle.

Equations (4) and (5) are written as a nonlinear four-dimensional system, for the variables $\mathbf{V}=(u_p,v_p)$ and $\mathbf{x}_p=(x_p,y_p)$.[21] Without any loss of generality we can restrict the mathematical formulation to the case when gravity points in the negative y direction. With these considerations, the system is written as

$$\dot{\mathbf{x}}=\mathbf{F}(\mathbf{x}), \tag{8}$$

where

$$\mathbf{x}=\begin{Bmatrix}x_p\\y_p\\u_p\\v_p\end{Bmatrix}\quad \mathbf{F}(\mathbf{x})=\begin{Bmatrix}u_p\\v_p\\\frac{1}{\mathrm{St}}(u_f-u_p)\\\frac{1}{\mathrm{St}}(v_f-v_p)-\frac{1}{\mathrm{Fr}^2}\end{Bmatrix}. \tag{9}$$

The system of equations (8) and (9) with initial conditions $\{x_p,y_p,u_p,v_p\}$ specified at time $t=0$ constitute a nonlinear non-Hamiltonian dynamical system.

III. PARTICLE DYNAMICS IN THE ABSENCE OF GRAVITY

A. Equilibrium points and trajectories

The flow model, as defined by Eqs. (3), provides only one equilibrium point for a particle, in the absence of gravity, at the center of the vortex. By equilibrium point we mean a location where the particle has zero velocity and acceleration, all forces considered to act upon it being perfectly balanced. In the following we analyze the linear stability of this equilibrium point. The plane velocity field (3) is linearized around the vortex center

$$u=-Ax-\frac{y}{4\pi}+O(r^2),$$
$$v=-Ay+\frac{x}{4\pi}+O(r^2), \tag{10}$$

and thus Eqs. (8) and (9) can be written as follows:

$$\begin{Bmatrix} \dot{x}_p \\ \dot{y}_p \\ \dot{u}_p \\ \dot{v}_p \end{Bmatrix} = \begin{Bmatrix} 0 & 0 & 1 & 0 \\ 0 & 0 & 0 & 1 \\ -b & -c & -a & 0 \\ c & -b & 0 & -a \end{Bmatrix} \begin{Bmatrix} x_p \\ y_p \\ u_p \\ v_p \end{Bmatrix}, \tag{11}$$

where

$$a=\frac{1}{\mathrm{St}}, \quad b=\frac{A}{\mathrm{St}}, \quad c=\frac{1}{4\pi\ \mathrm{St}}. \tag{12}$$

The coefficient matrix has complex eigenvalues of the form

$$s_{1,2,3,4}=-\frac{a}{2}\pm\frac{1}{2}\sqrt{a^2-4(b\pm ci)}. \tag{13}$$

For stability, one requires that the real parts of all of the eigenvalues be zero or negative. After isolating the real parts in (13) the inequality $\mathrm{Re}(s)\leqslant 0$ yields

$$c^2\leqslant a^2 b. \tag{14}$$

Replacing a, b, and c from (12) this condition gives a simple stability criterion for a particle moving in the vicinity of the vortex center. If St obeys

$$\mathrm{St}<16\pi^2 A=\mathrm{St}_{\mathrm{cr}}, \tag{15}$$

then the centrifugal force acting on the particle is always smaller than the inward radial drag force, hence the particle will be driven by the flow towards the center of the vortex. In the opposite situation, the centrifugal force overcomes the inward drag at small radii, thus the particle will move away from the vortex center and asymptotically approach a circular trajectory at a radius where the balance is restored due to increased inward fluid velocity.

By plotting the variation of the four eigenvalues given by (13), as shown in Fig. 1(a) for $A=0.003$, it is straightforward to verify that the periodic solution for the trajectory arises as a result of a Hopf bifurcation.[22] Two eigenvalues cross the imaginary axis as complex conjugates, while the other two have negative real parts.

By balancing the centrifugal and drag forces, we obtain for the radius of the trajectory

$$r^2\sqrt{\frac{A}{\mathrm{St}}}\frac{1}{2\pi}\left[1-\exp\left(-\frac{r^2}{2}\right)\right]=0. \tag{16}$$

The centrifugal and the drag forces on a particle moving along a circular trajectory of radius r depend on the radius, as shown in Fig. 1(b), for a St value higher than critical, where F_C and F_D stand for the centrifugal and drag force, respectively. From the plot, one can observe that the trajectory is unique and stable, as the two curves intersect in only one point, and any departure of the particle from the radius corresponding to the intersection point will generate an imbalance of the two forces which will drive the particle back towards the equilibrium trajectory. From this we can also conclude that the Hopf bifurcation is supercritical.

In order to obtain a feeling for typical particle sizes that might be trapped by the stretched, Burgers-like vortices observed at the small scales of turbulent flows, it is useful to

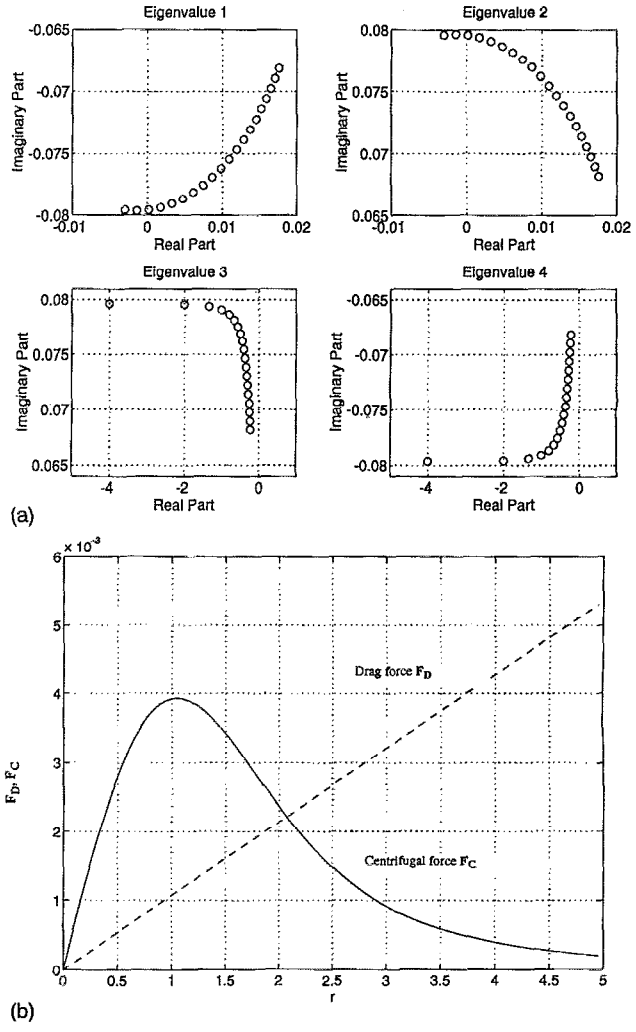

FIG. 1. (a) The variations of the four eigenvalues for $A=0.003$ and $0.001<\mathrm{St}<5.0$. Eigenvalues 1 and 2 cross the imaginary axis as complex conjugates, while eigenvalues 3 and 4 have negative real part. St values increase from left to right on each plot. (b) The variation of the centrifugal and inward drag forces acting on a particle characterized by St=2.8 moving along a circular trajectory around the center of a Burgers vortex with $A=0.003$, w.r.t. the radius of the trajectory (nondimensional), in the absence of gravity.

relate the above parameters to representative flow situations. From (6) and (15), using also $A=\nu/\Gamma$ we obtain

$$\frac{\mathrm{St}}{\mathrm{St}_{\mathrm{cr}}}=\frac{d^2}{288\pi^2}\frac{\rho_p}{\rho_f}\frac{\sigma}{\nu A^2}. \tag{17}$$

The direct numerical simulations of isotropic turbulence by Jiménez *et al.*[23] show that the core size $\delta=\sqrt{\nu/\sigma}$ of the Burgers-like intense vortical structures scales with the Kolmogorov scale η, and that typically $\delta/\eta=4$. Furthermore, the vortex Reynolds number A^{-1} scales approximately as

$$A^{-1}\sim 20\ \mathrm{Re}_\lambda^{1/2}, \tag{18}$$

where Re_λ is the Reynolds number formed with the Taylor microscale. Consequently, we obtain from (17):

$$\frac{\mathrm{St}}{\mathrm{St}_{\mathrm{cr}}}\sim 10^{-2}\frac{\rho_p}{\rho_f}\left(\frac{d}{\eta}\right)^2\mathrm{Re}_\lambda. \tag{19}$$

In the case of water droplets in air, $\rho_p/\rho_f=10^3$, thus

$$\frac{\mathrm{St}}{\mathrm{St_{cr}}}\sim 10\left(\frac{d}{\eta}\right)^2 \mathrm{Re}_\lambda . \tag{20}$$

For a typical laboratory experiment,[24] with $\mathrm{Re}_\lambda=190$ and $\eta=0.16$ mm, (20) gives $d_{cr}\approx 4$ μm.

A typical atmospheric flow,[25] on the other hand, is characterized by $\mathrm{Re}_\lambda\approx 10^4$ and $\eta=1$ mm, and from (20) we obtain again $d_{cr}\approx 4$ μm.

These estimates indicate that, as far as the small scale turbulent air flow is concerned, only small particles will be trapped. For other kinds of stretched vortex configurations, such as the streamwise structures observed in mixing layers,[26,27] we are currently evaluating the effect on the dynamics of heavy particles and droplets.

IV. GRAVITY EFFECTS

A. Equilibrium points

One immediately realizes that the equilibrium point at the center of the vortex will cease to exist in the presence of gravity. We will now determine if equilibrium is possible at other locations. In order to find equilibrium points, one has to solve Eqs. (8) and (9) for zero velocity and acceleration for the particle. The set (8) and (9) can be put in a condensed form of two second-order ODEs and one equation for r

$$\ddot{x}=\frac{1}{\mathrm{St}}\left\{-Ax-\frac{y}{2\pi(x^2+y^2)}\left[1-\exp\left(-\frac{x^2+y^2}{2}\right)\right]-\dot{x}\right\},$$

$$\ddot{y}=\frac{1}{\mathrm{St}}\left\{-Ay+\frac{x}{2\pi(x^2+y^2)}\left[1-\exp\left(-\frac{x^2+y^2}{2}\right)\right]-\dot{y}\right\}$$

$$-\frac{1}{\mathrm{Fr}^2}, \tag{21}$$

$$x^2+y^2=r^2.$$

By setting the particle velocity $\dot{x},\dot{y}$, and acceleration $\ddot{x},\ddot{y}$ to zero in (21) one can then solve for all the locations where equilibrium is achieved for the particle, stably or not. Eliminating x and y in favor of r, leads to a transcendental equation for r

$$r=\frac{\mathrm{St}}{\mathrm{Fr}^2 A}\frac{1}{\sqrt{1+\chi^2(r)}},\quad \text{where}\quad \chi(r)=\frac{1-\exp(-r^2/2)}{2\pi\,\mathrm{Ar}^2}. \tag{22}$$

Once we know the solutions for r we can immediately find the corresponding x and y coordinate values with

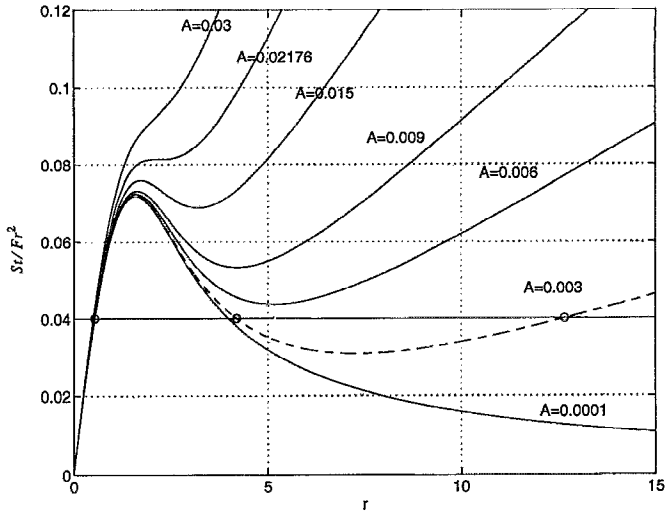

FIG. 2. Equilibrium curves. The intersection(s) of given $\mathrm{St/Fr^2}$ level line with an equilibrium curve corresponding to a given A parameter value yields the radial position of the equilibrium points of the particle within the flow field.

$$x=\frac{\mathrm{St}}{\mathrm{Fr}^2 A}\frac{\chi(r)}{1+\chi^2(r)},$$

$$y=-\frac{\mathrm{St}}{\mathrm{Fr}^2 A}\frac{1}{1+\chi^2(r)}. \tag{23}$$

From the way the parameters St, Fr, and A are grouped in Eqs. (22) and (23), the ratio $\mathrm{St/Fr^2}$ can be regarded as a single parameter. Physically, it expresses the terminal velocity a particle characterized by St would achieve if it were falling under the action of gravity in a still fluid. Therefore, Eq. (22) has two parameters, the terminal velocity $\mathrm{St/Fr^2}$ and the strain parameter A. In Fig. 2, the solutions to Eq. (22) are plotted versus the $\mathrm{St/Fr^2}$ values. The different equilibrium curves correspond to different values of the strain parameter A, as indicated. Such an equilibrium curve, intersected with a constant $\mathrm{St/Fr^2}$ line yields the radial position of the equilibrium locations, which can be multiple or unique. At the critical value $A_{cr}=0.021\,76$, a bifurcation from one unique solution to three solutions occurs. This equilibrium curve has a horizontal slope at the inflection point, as will be discussed below in more detail.

For illustration purposes, let us study the solutions for $\mathrm{St/Fr^2}=0.04$ and for $A=0.003$. Equation (22) states that there

TABLE I. Equilibrium radii for $A=0.003$, $\mathrm{St/Fr^2}=0.04$.

Radius	x	y	$\sqrt{\phi(r)}$	$\frac{A}{\lvert\phi(r)\rvert}=\mathrm{St_{cr}}$	Sign of $\phi(r)$
0.5397	0.5393	−0.0218	n/a	0.637 66	−
4.1906	3.9782	−1.3171	0.009 05	n/a	+
12.6547	3.9789	−12.0158	0.000 99	n/a	+

are three solutions for r, from which one can compute the coordinates of three equilibrium points using (23); see the first three columns in Table I.

B. Stability of the equilibrium positions

In order to determine if these equilibrium points are stable or not, we carry out a linear stability analysis. To this end, the fluid velocity field (3) is linearized around the generic location (x_0,y_0) of the equilibrium point under study. The initial position of the particle is displaced by a small distance (ϵ_x,ϵ_y) from the equilibrium position. By inserting $x=x_0+\epsilon_x$ and $y=y_0+\epsilon_y$ into (3) and retaining only the first-order terms in ϵ, we obtain the linearized velocity field in the vicinity of the equilibrium position (x_0,y_0):

$$
\begin{aligned}
u=&-Ax_0-A\epsilon_x-\frac{y_0}{2\pi r^2}\left[1-\exp\left(-\frac{r_0^2}{2}\right)\right]\\
&+\left(\frac{1-\exp(-r_0^2/2)}{\pi r_0^4}-\frac{\exp(-r_0^2/2)}{2\pi r_0^2}\right)x_0y_0\epsilon_x\\
&-\left[\frac{1-\exp(-r_0^2/2)}{2\pi r_0^2}-\left(\frac{1-\exp(-r_0^2/2)}{\pi r_0^4}\right.\right.\\
&\left.\left.-\frac{\exp(-r_0^2/2)}{2\pi r_0^2}\right)y_0^2\right]\epsilon_y,
\end{aligned}
\tag{24a}
$$

$$
\begin{aligned}
v=&-Ay_0-A\epsilon_y+\frac{x_0}{2\pi r_0^2}\left[1-\exp\left(-\frac{r_0^2}{2}\right)\right]\\
&+\left[\frac{1-\exp(-r_0^2/2)}{2\pi r_0^2}-\left(\frac{1-\exp(-r_0^2/2)}{\pi r_0^4}\right.\right.\\
&\left.\left.-\frac{\exp(-r_0^2/2)}{2\pi r_0^2}\right)x_0^2\right]\epsilon_x-\left\{\frac{1-\exp(-r_0^2/2)}{\pi r_0^4}\right.\\
&\left.-\frac{\exp(-r_0^2/2)}{2\pi r_0^2}\right\}x_0y_0\epsilon_y.
\end{aligned}
\tag{24b}
$$

We write Eqs. (8) and (9) for $x=x_0+\epsilon_x$ and $y=y_0+\epsilon_y$, using the velocity field (24), and then subtract from the resulting system the base equations, i.e., Eqs. (8) and (9) written for (x_0,y_0) and using the velocity field (3). The result of these algebraic manipulations is a system of four first-order ODEs with four unknowns, i.e., the particle's perturbed position (ϵ_x,ϵ_y) and velocity $(\epsilon_u=\dot{\epsilon}_x,\epsilon_v=\dot{\epsilon}_y)$

$$
\begin{Bmatrix}\dot{\epsilon}_x\\ \dot{\epsilon}_y\\ \dot{\epsilon}_u\\ \dot{\epsilon}_v\end{Bmatrix}=\begin{bmatrix}0&0&1&0\\0&0&0&1\\-b&-d&-a&0\\e&-c&0&-a\end{bmatrix}\begin{Bmatrix}\epsilon_x\\ \epsilon_y\\ \epsilon_u\\ \epsilon_v\end{Bmatrix},
\tag{25}
$$

where

$$
a=\frac{1}{\mathrm{St}},\quad b=\frac{A-f_1(r_0)}{\mathrm{St}},\quad c=\frac{A+f_1(r_0)}{\mathrm{St}},\quad d=\frac{f_2(r_0)}{\mathrm{St}},\quad e=\frac{f_3(r_0)}{\mathrm{St}}
\tag{26}
$$

and

$$
\begin{aligned}
f_1(r_0)&=\left(\frac{1-\exp(-r_0^2/2)}{\pi r_0^4}-\frac{\exp(-r_0^2/2)}{2\pi r_0^2}\right)x_0y_0,\\
f_2(r_0)&=\frac{1-\exp(-r_0^2/2)}{2\pi r_0^2}-\left(\frac{1-\exp(-r_0^2/2)}{\pi r_0^4}\right.\\
&\quad\left.-\frac{\exp(-r_0^2/2)}{2\pi r_0^2}\right)y_0^2,\\
f_3(r_0)&=\frac{1-\exp(-r_0^2/2)}{2\pi r_0^2}-\left(\frac{1-\exp(-r_0^2/2)}{\pi r_0^4}\right.\\
&\quad\left.-\frac{\exp(-r_0^2/2)}{2\pi r_0^2}\right)x_0^2.
\end{aligned}
\tag{27}
$$

The coefficient matrix of the system (25) has eigenvalues of the form

$$
s_{1,2,3,4}=-\frac{1}{2\ \mathrm{St}}\pm\frac{1}{2}\sqrt{\frac{1}{\mathrm{St}^2}-\frac{4A}{\mathrm{St}}\pm\frac{4}{\mathrm{St}}\sqrt{f_1^2(r_0)-f_2(r_0)f_3(r_0)}},
\tag{28}
$$

thus the discussion of stability depends on the value of the expression

$$
\begin{aligned}
\phi(r_0)&=f_1^2(r_0)-f_2(r_0)f_3(r_0)\\
&=\left(\frac{1-\exp(-r_0^2/4)}{2\pi r_0^2}\right)\left(\frac{1-\exp(-r_0^2/2)}{2\pi r_0^2}\right.\\
&\quad\left.-\frac{\exp(-r_0^2/2)}{2\pi}\right).
\end{aligned}
\tag{29}
$$

First, if $\phi(r_0)$ is negative, all four eigenvalues are complex. Their real parts have the expression

$$
\mathrm{Re}(s)=-\frac{1}{2\ \mathrm{St}}\pm\frac{1}{2}\rho^{1/2}\cos\left(\frac{\theta}{2}\right),
$$

where

$$
\rho^2=\frac{(1-4A\ \mathrm{St})^2}{\mathrm{St}^4}+\frac{16|\phi(r_0)|}{\mathrm{St}^2}
$$

and

$$
\theta=a\tan\left(\frac{4\ \mathrm{St}\sqrt{|\phi(r_0)|}}{(1-4A\ \mathrm{St})}\right).
\tag{30}
$$

For stability, one requires that $\mathrm{Re}(s)\leq 0$, which leads to the stability condition,

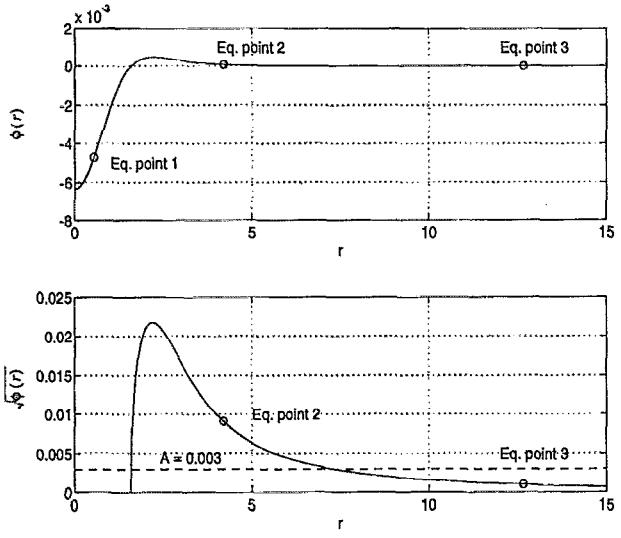

FIG. 3. Variation of $\phi(r)$ and its square root (when positive) with the radius. The radial locations for the equilibrium points marked, correspond to the case when $\mathrm{St}/\mathrm{Fr}^2=0.04$ and $A=0.003$.

$$\mathrm{St} \leqslant \frac{A}{|\phi(r_0)|} = \mathrm{St}_{cr}. \tag{31}$$

Therefore, stability in this case depends explicitly on St and A but not on the parameter $\mathrm{St}/\mathrm{Fr}^2$. The dependence on the last parameter is implicit, since its value determines the position.

Second, when $\phi(r_0) \geqslant 0$, the eigenvalues may be either real or complex depending on the whole expression under the outer square root in (28);

$$\psi = \frac{1}{\mathrm{St}^2} - \frac{4A}{\mathrm{St}} \pm \frac{4}{\mathrm{St}} \sqrt{\phi(r_0)} \tag{32}$$

being positive or negative, respectively. In this case, complex eigenvalues indicate stability, since the real part left is negative. For real eigenvalues stability requires that the largest eigenvalue be negative or zero. Analyzing (28), one obtains stability if $\psi \leqslant 1/\mathrm{St}^2$ and instability is $\psi > 1/\mathrm{St}^2$. This immediately results in stability if $A \geqslant \sqrt{\phi(r_0)}$ and instability if $A < \sqrt{\phi(r_0)}$.

Therefore, in summary, the conditions for stability of an equilibrium position located at a certain radius r_0 are

$$\phi(r_0) < 0 \begin{cases} \mathrm{St} \leqslant \dfrac{A}{|\phi(r_0)|} & \text{stable,} \\ \mathrm{St} > \dfrac{A}{|\phi(r_0)|} & \text{unstable,} \end{cases} \tag{33a}$$

$$\phi(r_0) > 0 \begin{cases} A \geqslant \sqrt{\phi(r_0)} & \text{stable,} \\ A < \sqrt{\phi(r_0)} & \text{unstable.} \end{cases} \tag{33b}$$

Examining the curves in Fig. 3, which show the variation of $\phi(r)$ and $\sqrt{\phi(r)}$ vs r, one can observe that the first condition in (33) applies to equilibrium positions located at small radii, in the proximity of the vortex center. The second condition applies to equilibrium positions located at larger radii, where the stability criterion does not explicitly depend on St, but only implicitly, through the value of the radius r at these locations. For all equilibrium points, there is no explicit dependence of their stability on Fr, only an implicit one, as the position itself depends on Fr.

An analysis of the particular set of equilibrium positions shown in Table I will provide a better understanding of our results. Here we consider three cases: In the first case, $A=0.003$, $\mathrm{St}=0.5$, and $\mathrm{Fr}=3.5355$; In the second case, $A=0.003$, $\mathrm{St}=1.0$, and $\mathrm{Fr}=5.0$; and in the third case, $A=0.003$, $\mathrm{St}=10.0$, and $\mathrm{Fr}=15.811\,38$. The parameters are chosen such that $\mathrm{St}/\mathrm{Fr}^2$ and A values are the same in all three cases, thus the equilibrium positions are the same.

Applying the set of stability conditions (33) and using the values in Table I, one can predict that the equilibrium point 1 is stable in the first case and unstable in the second and third cases. The equilibrium points 2 and 3 are unstable and stable, respectively, for all three cases. The stability of the equilibrium point 1 depends on St and a comparison of the values in the three cases with the critical value in Table I yields the nature of the point. In Fig. 3, one can observe that, for all three cases, the necessary stability condition $\sqrt{\phi(r)} \leqslant A$ is not satisfied for the equilibrium point 2, and satisfied for the equilibrium point 3.

In Fig. 4, numerical simulations for the three cases considered are shown. The vortex center is located at (0,0). In each simulation, 50 particles are initially seeded along the line $y=-x$ starting from a location (0.01, 0.01), and placed at regular intervals $\Delta r=0.35$ with zero initial velocity. These initial conditions were selected for purely illustrative purposes, as they provide a clear pattern of the particle trajectories. The successive positions of each particle are then tracked in time using a fourth-order Runge–Kutta algorithm, and plotted. In Fig. 4(a), the particles in the upper region are spiraling into the first equilibrium position, while the rest of them are attracted by the third equilibrium point. No accumulation is observed at the middle (second) equilibrium point. In Fig. 4(b), corresponding to the second case, the particles in the upper region do not accumulate at the first equilibrium point which is no longer stable, however, they orbit it along a closed, stable trajectory. The rest of the particles collect at the third equilibrium point, while, again, no accumulation occurs at the middle point. In Fig. 4(c), the particles' St is much larger than St_{cr} for stability at the first equilibrium position, and even orbiting the point is no longer possible. All particles collect at the third equilibrium point.

The nature of the multiple equilibrium points can be better explained by plotting a directional force-field graph. The directional force field is computed by setting the particle velocity $\dot{x},\dot{y}$ to zero in (21), then computing the values of the right-hand side terms of the resulting equations at each point (x,y) of the graph. By tracking marker particles moving in the resulting force field, one can obtain a directional graph of the force lines similar to the streamlines in a flow field. Physically, the value of the force field at a certain location (x,y) gives the magnitude of the force which would act on a particle if the particle were kept fixed at that position. The

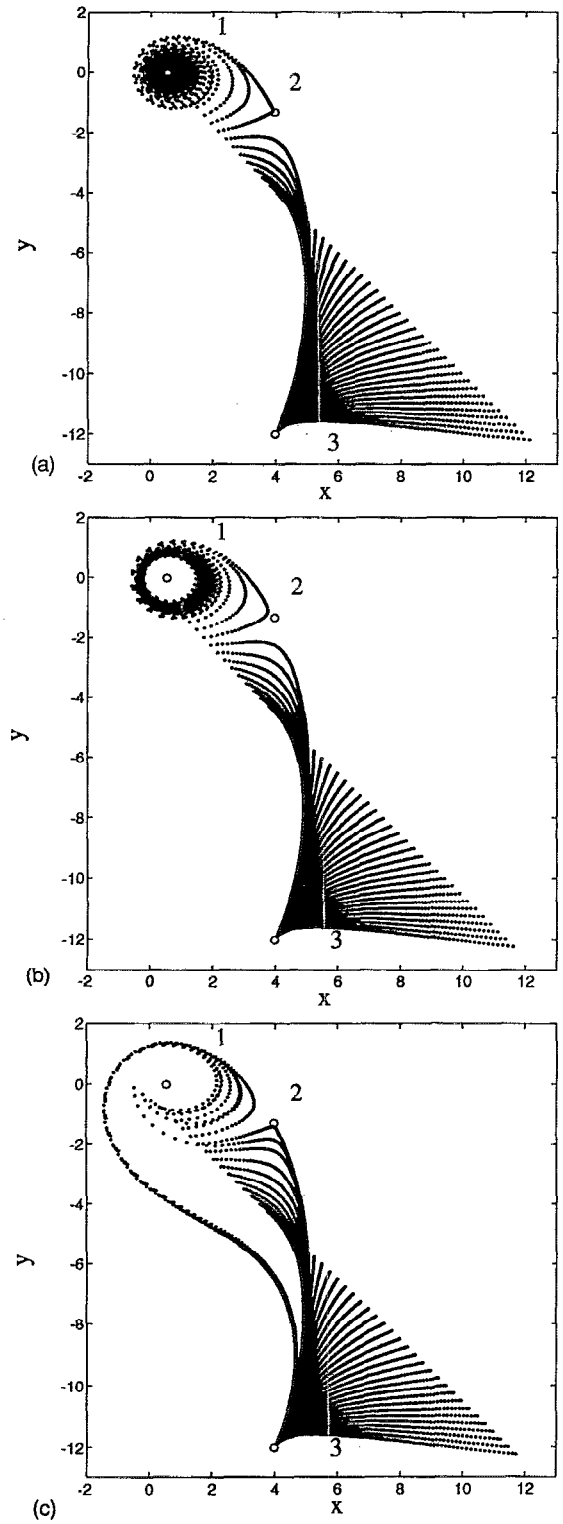

FIG. 4. Particle trajectories for the case $St/Fr^2=0.04$ and $A=0.003$. (a) St=0.5, Fr=3.5355. (b) St=1.0, Fr=5.0. (c) St=10.0, Fr=15.8114.

equilibrium points will then be stagnation points in this graph since equilibrium points are given by zeros in the force field. Another physical interpretation is also useful in analyzing the resulting plots. The right-hand side terms in (21), with the particle velocity $\dot{x},\dot{y}$ set to zero, can be written as

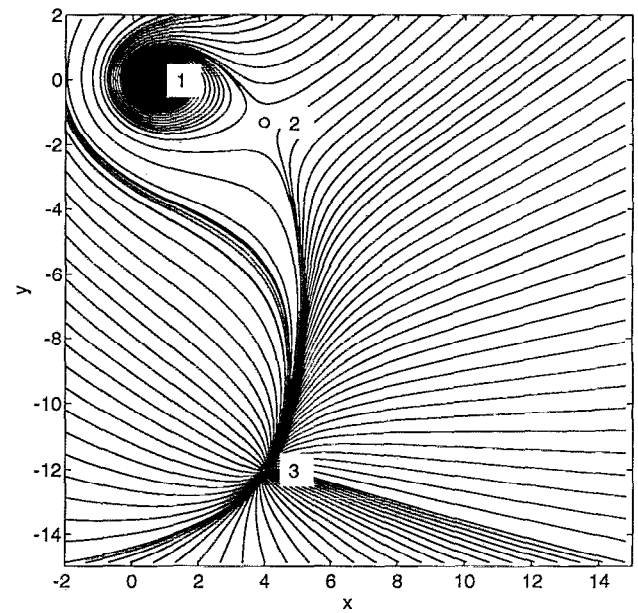

FIG. 5. Directional force field graph for the case $\{A, St/Fr^2\}=\{0.003,0.04\}$.

$$\mathscr{V}_x=\frac{1}{St}\left\{-Ax-\frac{y}{2\pi r^2}\left[1-\exp\left(-\frac{r^2}{2}\right)\right]\right\},$$
$$\mathscr{V}_y=\frac{1}{St}\left[-Ay+\frac{x}{2\pi r^2}\left(1-\exp\left(-\frac{r^2}{2}\right)\right)-\frac{St}{Fr^2}\right], \tag{34}$$

which is the initial velocity field (3) generated by the Burgers vortex, from which the terminal velocity of the particle St/Fr^2 has been subtracted, then multiplied by a 1/St factor. Equations (34) can be viewed as a modified velocity field $(\mathscr{V}_x,\mathscr{V}_y)$ within, which the particles will move without gravity.

The directional force field graph for the parameter set considered in Table I is shown in Fig. 5. The graph clearly shows the nature of the three equilibrium points. The equilibrium point 1, located closest to the center of the vortex is a focus, with the stability given by (33) for $\phi(r)<0$. The middle equilibrium point is a saddle, therefore unstable, while the last, equilibrium point 3, is a node, thus stable.

The influence of the strain parameter A and the terminal velocity St/Fr^2 on the existence and stability nature of the equilibrium point can also be explained by using the directional force field graphs.

Using the parameter set $A=0.003$ and $St/Fr^2=0.04$ as reference case, the effect of increasing A is shown in Fig. 6. In Fig. 6(a), A is increased from 0.003 to 0.005. There are still three equilibrium points, with the same stability properties, but the saddle point is located very close to the node (refer, also, to Fig. 2). In Fig. 6(b), for $A=0.006$ there is only one equilibrium point left, the focus. Between $A=0.005$ and $A=0.006$ the saddle and the node have merged and then vanished.

The effect of increasing St/Fr^2 is shown in Fig. 7 for a fixed value of $A=0.003$, by comparison to the same refer-

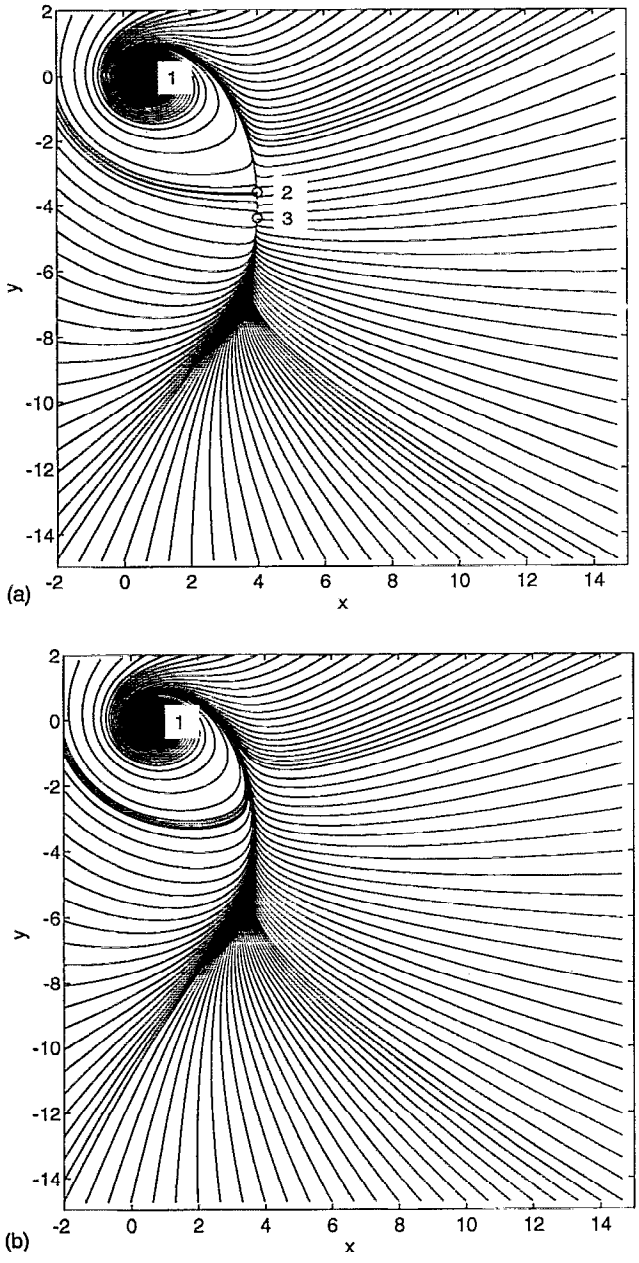

FIG. 6. Directional force field graphs. Dynamics of the equilibrium points at constant level of terminal velocity $St/Fr^2=0.04$, with increasing strain parameter A values. (a) $A=0.005$, $St/Fr^2=0.04$. Three equilibrium points still exist. The equilibrium point 2, the saddle, is closer to the equilibrium point 3, the node. (b) $A=0.006$, $St/Fr^2=0.04$. Unique equilibrium point, the focus. The node and the saddle have merged and vanished.

ence case. In Fig. 7(a), St/Fr^2 is increased to 0.055. There are still three equilibrium points, with the same stability properties, but we observe a repositioning: the saddle is closer to the focus, while the node has relocated to a larger radius (see, also, Fig. 2, and find the intersections of the level line $St/Fr^2=0.055$ with the equilibrium curve corresponding to $A=0.003$). Also, the inward spiraling force field around the focus is less vigorous. In Fig. 7(b), St/Fr^2 has been increased to 0.073. In this case, there is only one equilibrium point left, the node. The focus and the saddle have merged and vanished.

As the curves shown in Fig. 2 suggest, there is a maximum value of A above which multiple equilibrium points can no longer exist. For values of A larger than this critical value, a line $St/Fr^2=$const will no longer intersect the curve $St/Fr^2 = f(r)|_{A=A_0}$ in three points but only in one, no matter what the const value is. For critical A, the curve $St/Fr^2 = f(r)|_{A=A_{cr}}$ has an inflection point at the same location where the slope is zero. For the St/Fr^2 value corresponding to that location, all three equilibrium points observed for lower A have merged into only one. The critical value for A can be obtained by writing the equation of a curve St/Fr^2

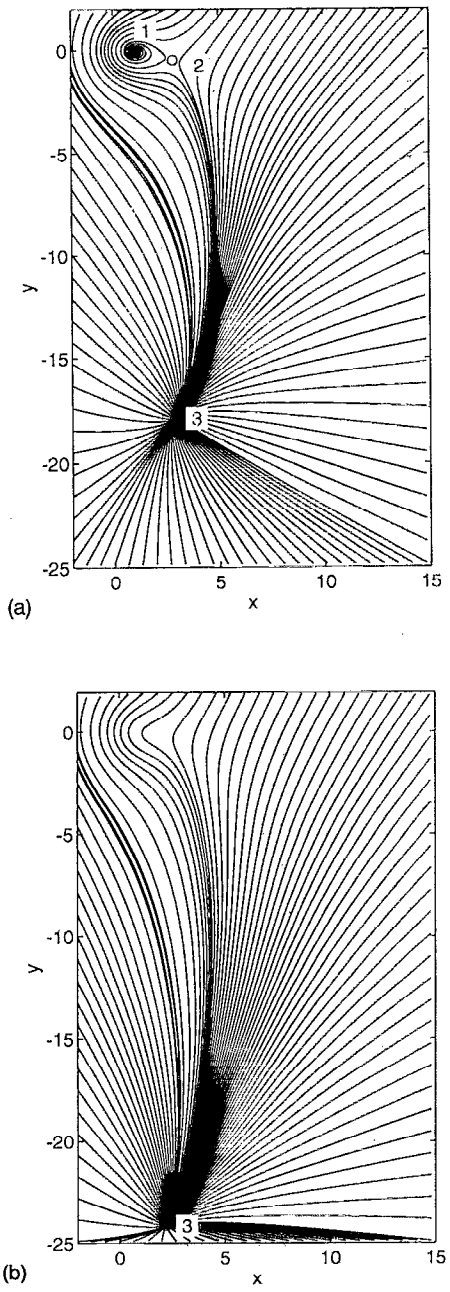

FIG. 7. Directional force field graphs. Dynamics of the equilibrium points at constant strain parameter A value, with increasing terminal velocity St/Fr^2. (a) $A=0.003$, $St/Fr^2=0.055$. Three equilibrium points exist. Equilibrium point 2, the saddle, is closer to the equilibrium point 1, the focus. (b) $A=0.003$, $St/Fr^2=0.073$. Unique equilibrium point, the node. Equilibrium points 1 and 2 have merged and vanished.

$= f(r)|_{A=A_0}$ using the equilibrium equation (22), and then requiring the first and second derivatives with respect to the radius of this curve be zero. Based on Eq. (22), one can write

$$\frac{\mathrm{St}}{\mathrm{Fr}^2}=\mathrm{Ar}\sqrt{1+\left(\frac{[1-\exp(-r^2/2)]}{2\pi r^2 A}\right)^2} \tag{35}$$

which expresses the variation of the terminal velocity $\mathrm{St/Fr}^2$ with the radius, while A is a parameter. For different values of A, Eq. (35) gives the curves in Fig. 2. Based on (35), the conditions for the critical A are

$$\frac{d}{dr}\left(\frac{\mathrm{St}}{\mathrm{Fr}^2}\right)=0,$$
$$\frac{d^2}{dr^2}\left(\frac{\mathrm{St}}{\mathrm{Fr}^2}\right)=0. \tag{36}$$

Equations (36) form a system of two equations with two unknowns, A and r. The equations have a transcendental form, allowing only for a numerical solution. Using Mathematica™, we have found the critical value $A_{cr}=0.021\,76$. The location of the triple equilibrium point corresponding to this A value, is (see Fig. 2) $r=2.1866$ and $\mathrm{St/Fr}^2=0.0815$.

For values of A smaller than A_{cr} there will always exist three equilibrium points within a range of $\mathrm{St/Fr}^2$ values delimited by the local maximum and the local minimum of an equilibrium curve like the ones shown in Fig. 2. The size of this range depends on the actual value of A. The stability of these points is given by (33). One can note that the stability conditions (33) differ qualitatively for positive and negative values of $\phi(r)$. The change in sign occurs at $r=1.5852$ where $\phi(r)=0$. One can find for every A value, the terminal velocity level $\mathrm{St/Fr}^2=$const which determines the equilibrium point location at exactly $r=1.5852$ In order to find this terminal velocity level, simply substitute the desired A, and $r=1.5852$ in (35). The pair of A and $\mathrm{St/Fr}^2$ computed this way characterizes the transition in the stability nature of equilibrium point 1, which will be explained below.

The significance of these values is explained in Fig. 8, where the transition curve is shown. For $\mathrm{St/Fr}^2$ values above the transition curve, the equilibrium point(s)' stability no longer depends explicitly on the St. The qualitative change occurs for the equilibrium point located closest to the center of the vortex: it changes from a focus to a node as soon as its location exceeds $r=1.5852$. This process occurs for multiple or unique equilibrium point cases but it always concerns the first point in the multiple case. We will present here the transition for an equilibrium point located on a curve with $A>A_{cr}$, on which the equilibrium point is unique for any given $\mathrm{St/Fr}^2$ level.

Figure 9 shows the directional force field for an equilibrium point located at successively outward positions—and therefore at successively higher $\mathrm{St/Fr}^2$ levels—along the $A=0.03$ equilibrium curve. In Fig. 9(a), the equilibrium point is located at a radius $r=0.4959$ corresponding to a level $\mathrm{St/Fr}^2=0.04$. At this radius $\phi(r)$ is negative, thus the stability depends explicitly on St according to stability condition (31). The directional force field lines display a spiraling pattern around the equilibrium point, which explains the

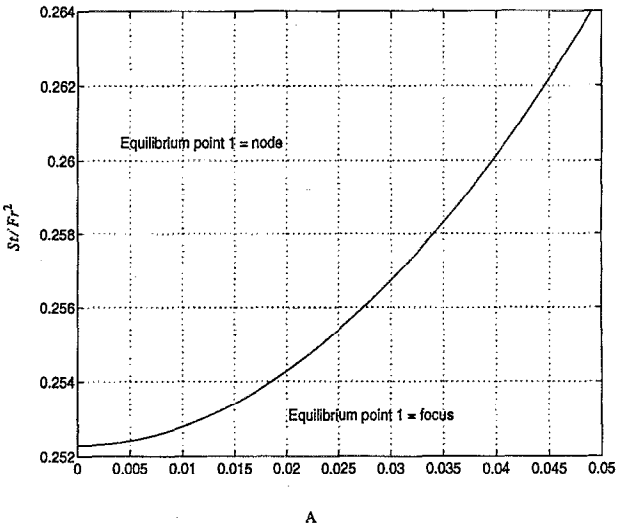

FIG. 8. Transition curve: variation of the terminal velocity $\mathrm{St/Fr}^2$ at which the equilibrium point 1 changes its stability nature from a focus into a node versus the strain parameter A.

nature of the stability at that point: a particle approaching the equilibrium position will undergo an angular acceleration, thus, if possessing enough inertia it will be expelled or kept along a closed trajectory by the centrifugal force. In Fig. 9(b), the equilibrium point is located at a radius $r=1.3004$, corresponding to a level $\mathrm{St/Fr}^2=0.08$. Again, $\phi(r)$ is negative, however, its modulus is very small, thus giving a large value $\mathrm{St}_{cr}=32.2016$, hence large range of St values for which the point is stable. Nevertheless, when the equilibrium point is located at a radius $r=2.7484$, which corresponds to a level $\mathrm{St/Fr}^2=0.1$, as shown in Fig. 9(c), $\phi(r)$ is positive, and the stability at this point no longer depends explicitly on St. As the directional force field line patterns suggest, any particle within a vicinity of the equilibrium point will be steadily driven towards the equilibrium point, which has become a node.

We can again evaluate the applicability of the above results by relating them to the small scale turbulent structures in representative laboratory and atmospheric flow situations. As Fig. 2 shows, multiple equilibrium solutions are possible only for $A<0.021\,76=A_{cr}$, i.e., approximately for vortex Reynolds numbers $\mathrm{Re}_\gamma=\Gamma/\nu\geqslant 50$. Using the scaling relation (18), we obtain $\mathrm{Re}_\lambda\geqslant 6$. This indicates that both for atmospheric and for laboratory turbulent flows the vortex Reynolds numbers of the small-scale-stretched vortices are sufficiently large for multiple solutions to exist. As far as the particles themselves are concerned, we see from Fig. 2 that they must satisfy $\mathrm{St/Fr}^2\leqslant 0.0815$ in order to allow for multiple solutions. Using (6) and (7), we obtain for $\rho_p\gg\rho_f$

$$\frac{\mathrm{St}}{\mathrm{Fr}^2}=\frac{d^2}{18}\frac{\rho_p}{\rho_f}\frac{g}{\nu^2}\,\delta A\leqslant 0.0815. \tag{37}$$

It should be noted here that g is the projection of the gravitational acceleration in the r, θ plane, $\mathrm{St/Fr}^2$ will be

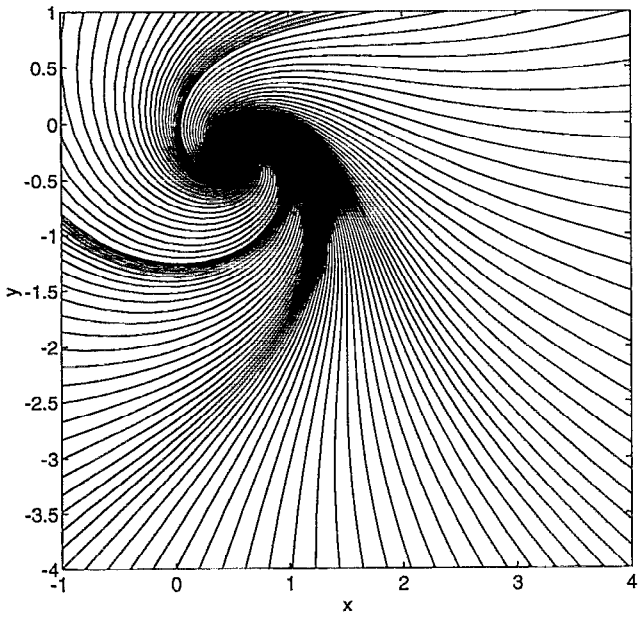

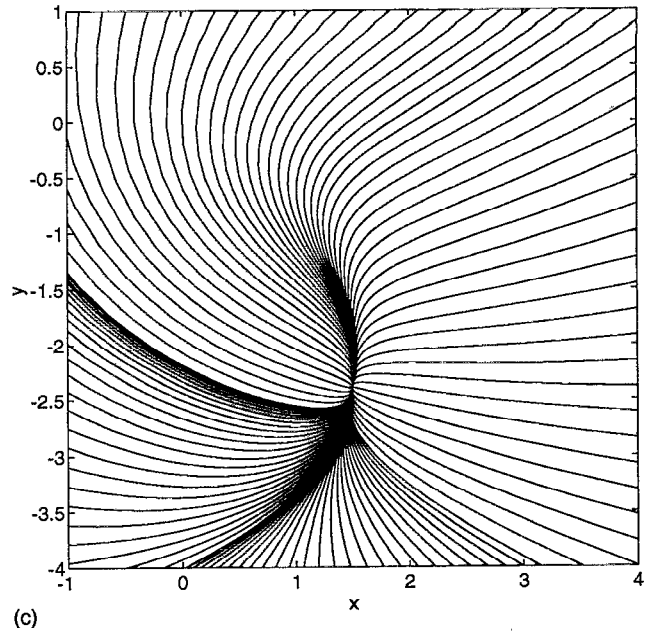

(c)

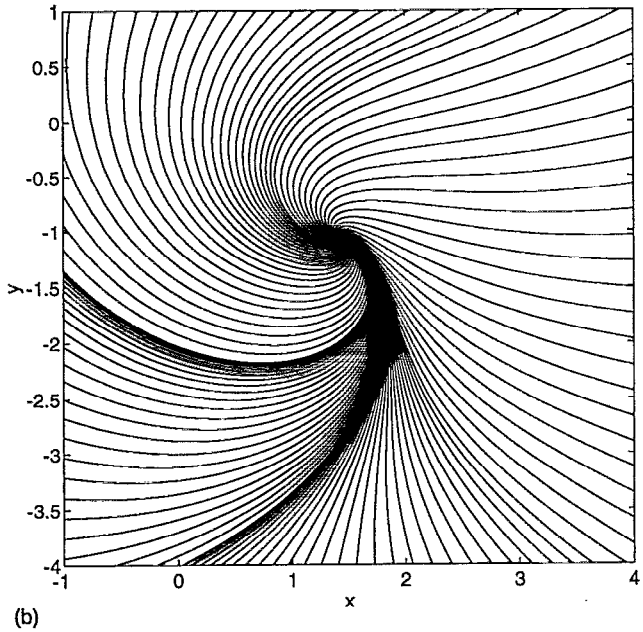

(b)

FIG. 9. Directional force field graphs. The change in nature of a unique equilibrium point at constant strain parameter A value, with increasing terminal velocity $\mathrm{St}/\mathrm{Fr}^2$. (a) $A=0.03$, $\mathrm{St}/\mathrm{Fr}^2=0.04$. The equilibrium point is a focus. (b) $A=0.03$, $\mathrm{St}/\mathrm{Fr}^2=0.08$. The equilibrium still remains a focus, however, the spiraling of the directional force lines is weak. (a) $A=0.03$, $\mathrm{St}/\mathrm{Fr}^2=0.1$. The equilibrium point is a node.

largest for horizontal vortices. For water droplets in air, $\rho_p/\rho_f=10^3$ and $g/\nu^2\approx 5\times 10^{10}$ m^{-3}, thus the condition (37) becomes

$$d^2\delta A \leqslant 3\times 10^{-14}\ \mathrm{m}^3.$$

With the scaling relation (18), this leads to

$$d^2 \leqslant \frac{6\times 10^{-13}\ \mathrm{m}^2}{\delta}\,\mathrm{Re}_\lambda^{1/2}.$$

Using again $\delta=4\eta$ and the the Browne *et al.*[24] data for typical laboratory flow, i.e., $\eta=0.16\times 10^{-3}$ m and $\mathrm{Re}_\lambda=190$, the critical particle diameter becomes $d_{\mathrm{cr}}\approx 115$ μm, while for atmospheric flows, using the Wyngaard[25] data, $\delta=4\eta=4\times 10^{-3}$ m, and $\mathrm{Re}_\lambda=10^4$, we obtain $d_{\mathrm{cr}}\approx 120$ μm.

In a spray with a size distribution similar to that observed by Lázaro and Lasheras,[5] we would hence expect the largest droplets to fall into the single solution regime. Most of the droplets, however, would be in the multiple solution regime, where the outermost solution is always stable and the middle one always unstable, with the stability of the nearest solution depending on the exact parameters of the flow.

V. CONCLUSIONS

We have presented a linear stability analysis as well as some numerical results for the motion of heavy particles in the flow field of a Burgers vortex. The findings are expected to be applicable to the coupling between the small scales of a turbulent fluid velocity field and the motion of heavy particles suspended in the flow. We consider only the effects of particle inertia, Stokes drag, and gravity, so that we obtain as the governing equations for the particle motion a four-dimensional nonlinear dissipative system with three dimensionless parameters, namely the particle Stokes number, a Froude number, and a vortex strain parameter.

The results show that in the absence of gravity, sufficiently light particles can be stably located at the vortex center, since the inward drag force created by the strain field is strong enough to overcome the destabilizing centrifugal force on the particle. The critical value of the Stokes number for instability is given analytically. A particle with a Stokes number larger than the critical value orbits the center of the vortex along a circular trajectory, whose radius is a function of both Stokes number and strain parameter.

When the effect of gravity is considered as well, the vortex center no longer is an equilibrium point, and instead either one or three equilibrium points appear away from the center. The location of these equilibrium points depends on the terminal settling velocity and the strain parameter. If the strain parameter is smaller than a critical value, three equilibrium points exist within a certain range of terminal settling velocities, otherwise, there is only one equilibrium point. Near the vortex center, the stability depends on both Stokes number and strain parameter, while farther away from the center, only the strain parameter enters into the stability criterion. It should be mentioned that both the Stokes and the Froude number of course enter implicitly by determining the location of the equilibrium points. By analyzing the critical points of a related directional force field, we were furthermore able to relate changes in the stability properties of the equilibrium points to changes in the nature of the critical points.

ACKNOWLEDGMENTS

This work has been supported by the National Science Foundation under Grant No. CTS-9058065 and by the Electric Power Research Institute.

[1]C. T. Crowe, R. Gore, and T. R. Troutt, "Particle dispersion by coherent structures in free shear flows," Part. Sci. Tech. **3**, 149 (1985).
[2]J. N. Chung and T. R. Troutt, "Simulation of particle dispersion in an axisymmetric jet," J. Fluid Mech. **186**, 199 (1988).
[3]J. E. Martin and E. Meiburg, "The accumulation and dispersion of heavy particles in forced two-dimensional mixing layers. I. The fundamental and subharmonic cases," Phys. Fluids **6**, 1116 (1994).
[4]B. J. Lázaro and J. C. Lasheras, "Particle dispersion in a turbulent, plane, free shear layer," Phys. Fluids A **1**, 1035 (1989).
[5]B. J. Lázaro and J. C. Lasheras, "Particle dispersion in the developing free shear layer. Part 1. Unforced flow," J. Fluid Mech. **235**, 143 (1992a).
[6]B. J. Lázaro and J. C. Lasheras, "Particle dispersion in the developing free shear layer. Part 2. Forced flow," J. Fluid Mech. **235**, 179 (1992b).
[7]E. K. Longmire and J. K. Eaton, "Structure of a particle-laden round jet," J. Fluid Mech. **236**, 217 (1992).
[8]S. Elghobashi and G. C. Truesdell, "Direct simulation of particle dispersion in a decaying isotropic turbulence," J. Fluid Mech. **242**, 655 (1992).
[9]S. Elghobashi and G. C. Truesdell, "On the two-way interaction between homogeneous turbulence and dispersed solid particles. I. Turbulence modification," Phys. Fluids A **5**, 1790 (1993).
[10]G. C. Truesdell and S. Elghobashi, "On the two-way interaction between homogeneous turbulence and dispersed solid particles. II. Particle dispersion," Phys. Fluids **6**, 1405 (1994).
[11]K. D. Squires and J. K. Eaton, "Particle response and turbulence modification in isotropic turbulence," Phys. Fluids A **2**, 1191 (1990).
[12]K. D. Squires and J. K. Eaton, "Measurements of particle dispersion obtained from direct numerical simulations of isotropic turbulence," J. Fluid Mech. **226**, 1 (1991).
[13]K. D. Squires and J. K. Eaton, "Preferential concentration of particles by turbulence," Phys. Fluids A **3**, 1169 (1991).
[14]L.-P. Wang and M. R. Maxey, "Settling velocity and concentration distribution of heavy particles in homogeneous isotropic turbulence," J. Fluid Mech. **256**, 27 (1993).
[15]Z.-S. She, E. Jackson, and S. A. Orszag, "Intermittent vortex structures in homogeneous isotropic turbulence," Nature **344**, 226 (1990).
[16]G. R. Ruetsch and M. R. Maxey, "Small-scale features of vorticity and passive scalar fields in homogeneous isotropic turbulence," Phys. Fluids A **3**, 1587 (1991).
[17]W. T. Ashurst, "Is turbulence a collection of Burgers Vortices?" preprint (1991).
[18]J. M. Burgers, "A mathematical model illustrating the theory of turbulence," Adv. Appl. Mech. **1**, 171 (1948).
[19]T. Maxworthy, "Storm in a tea cup," J. Appl. Mech. **35**, 453 (1968).
[20]M. R. Maxey and J. J. Riley, "Equation of motion for a small rigid sphere in a nonuniform flow," Phys. Fluids **26**, 883 (1983).
[21]A. M. Gañán-Calvo and J. C. Lasheras, "The dynamics and mixing of small spherical particles in a plane, free shear layer," Phys. Fluids A **3**, 1207 (1991).
[22]J. K. Hale and H. Kocak, *Dynamics and Bifurcations* (Springer-Verlag, Berlin, 1991).
[23]J. Jiménez, A. A. Wray, P. G. Saffman, and R. S. Rogallo, "The structure of intense vorticity in isotropic turbulence," J. Fluid Mech. **255**, 65 (1993).
[24]L. W. B. Browne, R. A. Antonia, and N. Rajagopalan, "The spatial derivative of temperature in a turbulent flow and Taylor's hypothesis," Phys. Fluids **26**, 1222 (1983).
[25]J. C. Wyngaard, "Atmospheric turbulence," Annu. Rev. Fluid Mech. **24**, 205 (1992).
[26]W. T. Ashurst and E. Meiburg, "Three-dimensional shear layers via vortex dynamics," J. Fluid Mech. **189**, 87 (1988).
[27]L. P. Bernal and A. Roshko, "Streamwise vortex structure in plane mixing layers," J. Fluid Mech. **170**, 499 (1986).